Phases of granular segregation in a binary mixture

P. M. Reis,[1,*] T. Sykes,[2] and T. Mullin[2]
[1]*Laboratoire PMMH (UMR 7636 CNRS-ESPCI-P6-P7), 10 Rue Vauquelin, 75231 Paris, France*
[2]*Manchester Center for Nonlinear Dynamics, University of Manchester, Oxford Road, M13 9PL, United Kingdom*
(Received 30 May 2006; revised manuscript received 19 September 2006; published 15 November 2006)

We present results from an extensive experimental investigation into granular segregation of a shallow binary mixture in which particles are driven by frictional interactions with the surface of a vibrating horizontal tray. Three distinct phases of the mixture are established viz. binary gas (unsegregated), segregation liquid, and segregation crystal. Their ranges of existence are mapped out as a function of the system's primary control parameters using a number of measures based on Voronoi tessellation. We study the associated transitions and show that segregation can be suppressed as the total filling fraction of the granular layer, C, is decreased below a critical value, C_c, or if the dimensionless acceleration of the driving, γ, is increased above a value γ_c.

DOI: 10.1103/PhysRevE.74.051306 PACS number(s): 45.70.Mg, 45.70.Qj, 68.35.Rh

I. INTRODUCTION

Granular materials are ubiquitous in our everyday life, nature, and of crucial importance in industrial processes [1,2]. The study of granular media has a long tradition amongst engineers and geologists who have had successes in specific problems using a combination of practical experience and empirical knowledge. More recently the physics community has taken an increased interest in granular materials since they pose a number of fundamental questions which challenge current ideas in nonequilibrium statistical mechanics [3]. Interactions between granular particles are intrinsically dissipative since energy is lost due to both inelastic collisions and frictional contacts. Hence any dynamical study of a granular ensemble requires an energy input which typically takes the form of vibration or shear [4,5]. In this sense, detailed investigations of granular media provide examples of canonical systems where dynamical processes are far from equilibrium [6].

An interesting and counterintuitive feature of particulate matter is segregation of binary assemblies, where an initially uniform mixture of particles can spontaneously demix into its constituent components under flow [7]. Typically, the species of particles may differ in size, density, rigidity, or surface properties. Such differences can often lead to separation and hence clustering of like particles [8,9]. Intriguingly, segregation does not always happen and the conditions for its occurrence are difficult to predict. An extensive account of the issues involved can be found in the following reviews [10–13].

The phenomena has been recognized for a considerable period of time [14] but, despite more than half a century of research, the underlying nature of the mechanisms involved are not yet understood. Apart from posing various theoretical questions, insight into segregation would be beneficial for many applications. These include areas such as agriculture, geophysics, material science, and several branches of engineering, e.g., involving preparation of food, drugs, detergents, cosmetics, and ceramics [14]. In many of these examples the processing and transporting of mixtures can lead to undesired separation. Segregation of mixtures can be brought about by the simple actions of pouring, shaking, vibration, shear, and fluidization and is also found in industrial processes where the objective is to achieve particle mixing [8,15].

Over the last decade, significant interest in segregation has arisen in the physics community. A number of small scale laboratory experiments have been reported on vertically [16–20] and horizontally [21–24] vibrated beds, filling and emptying of vessels [25–28], and rotating cylindrical drums [26,29–32]. The spatial distribution and dynamics of segregation of large and small particles appears to depend on a number of factors besides size difference including density ratio, friction between particles, shape of boundaries, particle velocity, and the effects of the interstitial air. A great deal of research is required on the topic since the parameter space of such a system is large and seemingly trivial details turn out to have important effects on the segregation of mixtures. Designing simple and well-controlled laboratory based experiments and developing appropriate models is therefore essential to make progress in understanding segregation which in turn may give insights into the industrial problems outlined above.

We have recently developed an experiment to study the segregation of shallow layers of granular binary mixtures under horizontal vibration [33–36]. The existence and self-organization of three phases of segregation have been uncovered by systematically starting from homogeneous binary mixtures. These are, *binary gas* (unsegregated), *segregation liquid*, and *segregation crystal* and they exist over ranges of the total filling fraction of the layer, C. The principal result is the discovery of critical phenomena in the segregation process. This implies the existence of a transition point in C below which the layer remains mixed and above which segregation occurs. An overview of this work will be given in Sec. III.

In this paper we present the results of an extensive experimental investigation where we show that this phase behavior of the granular mixture is robust over a range of control parameter space. Moreover, we investigate the role of the driving on the segregation process and uncover an additional transition between the segregated and mixed phases as the

*Email address: preis@pmmh.espci.fr

dimensionless acceleration of the tray is increased. We perform particle tracking and use the distribution of positions of the centers of one of the particle types to define a number of measures derived from Voronoi tessellation to characterize the state of the mixture. This detailed study points to a robust behavior of our granular mixture which invites the development of a predictive theoretical model.

This paper is organized as follows. A description of the experimental apparatus is given in Sec. II. In Sec. III we describe the nature of segregation patterns observed in our system and briefly review some results from our previous work. The microscopic measures obtained from Voronoi tessellation, namely the local Voronoi density and the angle between nearest neighbors, are discussed in Secs. IV A and IV B. In Sec. V we report the results of an exploration of the parameter space of the system including the aspect ratio of the cell (Sec. V A), the filling fraction of the mixture (Sec. V B), and forcing parameters (Sec. V C). Finally, in Sec. VI we relate our experimental results with recent numerical simulations and draw some conclusions.

II. THE EXPERIMENT

A schematic diagram of the apparatus is presented in Fig. 1(a). The experimental setup consisted of a horizontal rectangular tray with dimensions $(x,y)=(180,90)$ mm. It was connected to an electromechanical shaker so that a mixture of granular particles placed on the tray was vibrated longitudinally. Individual particles in the granular layer were forced via stick-and-slip frictional contacts with the oscillating surface of the container. Different removable frames could be attached to the tray to make changes in size, shape, and aspect ratio.

The tray was mounted on a horizontal platform which was connected to a Ling LDS V409 electromechanical shaker. Its motion was constrained to be unidirectional by four lateral high precision linear bush bearings. The shaker was driven sinusoidally using a HP 33120A function generator and the resulting dynamic displacement and acceleration of the shaking bed were monitored by a linear displacement variable transformer (LVDT) and a PCB quartz shear piezoelectric accelerometer.

The granular mixture consisted of phosphor-bronze precision spheres and poppy seeds and photographs of representative particles are shown in Figs. 1(c) and 1(d). The poppy seeds were nonspherical ("kidney" shaped) with an average diameter of 1.06 mm, polydispersity of 17%, and a density of 0.2 g cm^{-3}. The phosphor-bronze spheres had a diameter of 1.50 mm, polydispersity of 3.0%, and a density of 8.8 g cm^{-3}. In addition to being nonspherical the poppy seeds had a considerably larger surface roughness than the spheres, which resulted in a stronger frictional interaction with the surface of the oscillating tray. This is evident from the series of ridges in the surface of the seeds, as shown in Fig. 1(d). Interestingly, qualitatively the same segregation behavior is found using a mixture of sugar balls and polystyrene beads [33]. Hence the phenomena reported here are also found with approximately spherical particles with similar densities. This emphasizes the point that mechanisms behind segregation are complex and simple differences in size, shape, density, etc. may be insufficient to provide an explanation for the observed behavior.

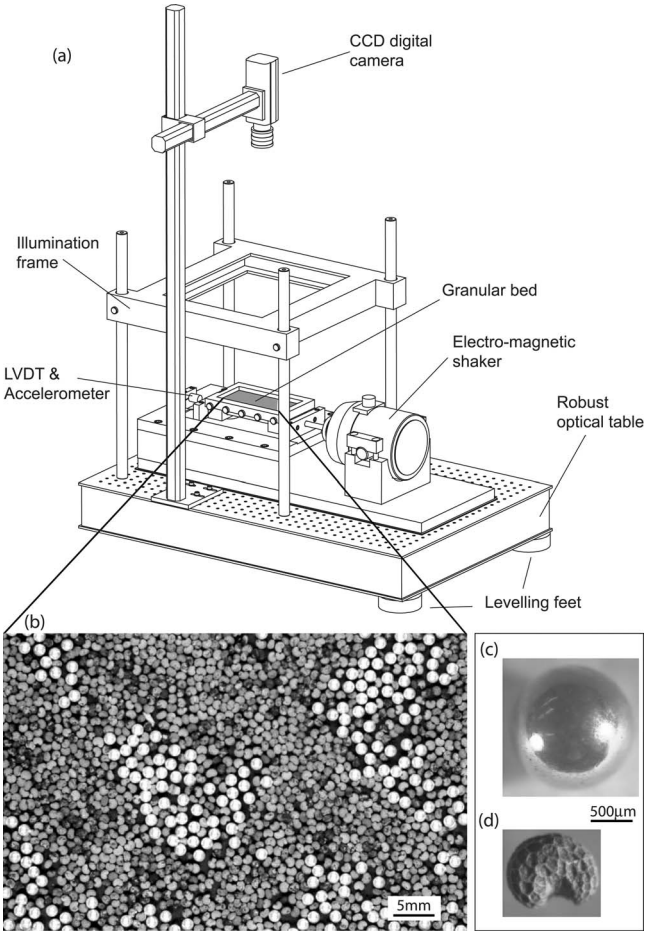

FIG. 1. The experimental setup. (a) Three-dimensional schematic diagram of the experimental apparatus. (b) Typical segregation patterns of the binary granular mixtures in the segregation liquid phase. Poppy seeds appear as dark gray regions and phosphor-bronze spheres as light gray. The frame was taken after 3 min of vibration from an initially homogeneous mixture ($C=0.708$, $\Gamma=2$, $f=12$ Hz, $A=\pm 1.74$ mm). (c) Photographs of a phosphor-bronze sphere and (d) a poppy seed.

We define the total filling fraction of the granular layer as

$$C(N_{ps},N_{pb}) = \frac{N_{ps}A_{ps} + N_{pb}A_{pb}}{xy} = \varphi_{ps} + \varphi_{pb}, \qquad (1)$$

where N_{ps} and N_{pb} are the numbers of poppy seeds (ps) and phosphor bronze spheres (pb) in the layer, $A_{ps}=(0.90\pm0.15)$ mm^2 and $A_{pb}=1.767$ mm$^2\pm0.028$ mm^2 are the two-dimensional projected areas of the respective individual particles and x and y are the longitudinal and transverse dimensions of the rectangular tray. φ_{ps} and φ_{pb} are the individual filling fractions for each of the particle species, respectively. Unless otherwise stated, C was varied by keeping the filling fraction of the spheres fixed at $\varphi_{pb}=0.174$ and changing the numbers of poppy seeds and thereby φ_{ps}. This enabled more controlled changes to be made in C but we also

investigated changes in both φ_{ps} and φ_{pb}, as will be discussed in Sec. V B.

In addition to the driving parameters and the total filling fraction, a geometrical dimensionless parameter, the *aspect ratio*, is defined as $\Gamma=\Delta x/\Delta y$ where Δx is the longitudinal length of the tray and Δy is the transverse width of the tray, perpendicularly to the direction of forcing. The values of Δx and Δy were changed using a variable frame which was positioned on all four sidewalls. Both Δx and Δy could be independently adjusted to the required value of Γ.

All experimental runs were performed in an *approximately monolayer regime*. The larger heavy phosphor-bronze spheres were always in a monolayer but the lighter and flatter poppy seeds could overlap. This degree of overlapping was due to both the polydispersity of the poppy seeds and the difference in size and shape between the poppy seeds and the spheres (size ratio of $q\sim 0.71$). The mixture was deemed to be in the *monolayer regime* if the extent of overlap of the poppy seeds was never such that the layer height exceeded the height corresponding to a diameter of the spheres. The failure of this criterion was readily noticed as smaller particles were observed to hop over domains of the larger particles. Hence for the highest values of the total filling fraction, C had values higher than those corresponding to maximum packing in two dimensions, which, for the case of monodisperse disks is $\pi/\sqrt{12}$. This choice of performing the experiments in this approximately monolayer regime has two advantages. First, particles are always in contact with the oscillatory surface of the tray, such that the forcing was provided homogeneously throughout the layer through frictional contacts. Second, these approximately two-dimensional experiments allowed the dynamics of the granular layer to be fully visualized by imaging the system from above.

All experimental runs were started using a homogeneous mixture as initial conditions. This was achieved using the following procedure. A particular filling fraction of N_{ps} poppy seeds was first vibrated at large amplitude, $A\sim\pm 5$ mm which created a homogeneous and isotropic layer. The phosphor-bronze spheres were then suspended above the layer, on a horizontal perforated plate with $(m\times n)$ 2 mm diameter holes arranged in a triangular lattice and held by a shutter on an independent superposed frame. The shutter was then opened and the $N_{pb}=m\times n$ phosphor-bronze spheres fell onto the layer of poppy seeds, creating a near homogeneous mixture of the two types of particles. An example of such an initial configuration is presented in Fig. 2(a). We found that if this procedure was not adopted, random initial clusters in a poorly prepared mixture could bias the results.

The dynamics of the segregation process were visualized using a near homogeneous illumination of the tray and the behavior monitored from above using a charge coupled device camera as shown in Fig. 1(a). Phosphor-bronze has a high reflection coefficient compared to the poppy seeds and the spheres appeared as sharp bright regions so that direct observation of their motion was relatively straightforward. The individual positions of the phosphor-bronze spheres were obtained in a central (73.1×59.5) mm^2 visualization window of the full granular layer in order to achieve the necessary resolution to obtain good estimates of the centers of the spheres. The spatial distribution of the positions of the phosphor-bronze spheres were obtained using image processing and particle tracking techniques which were then used to calculate a variety of measures. No tracking was carried out on the poppy seeds.

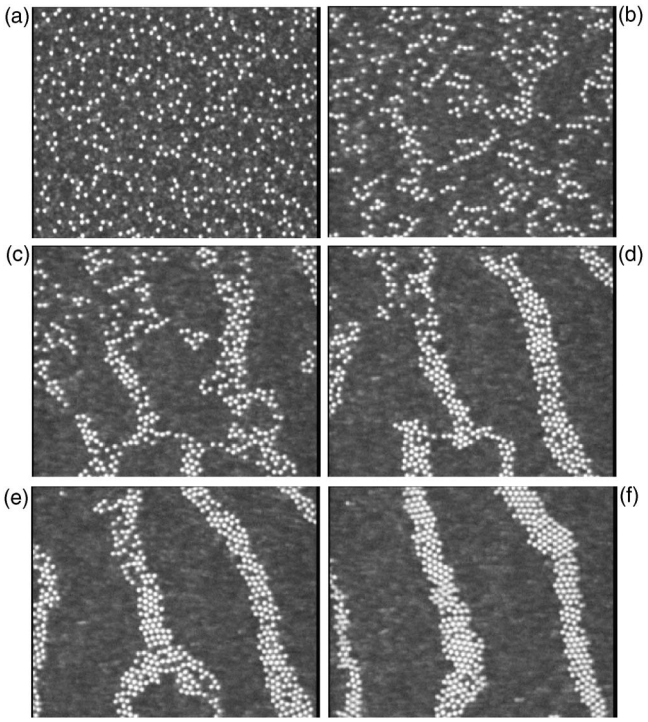

FIG. 2. Snapshots of the evolution of segregation domains in a mixture with $C=0.996$, $f=12$ Hz, $A=\pm 1.74$ mm (a) $t=0$ s—vibration of the granular layer was initiated from a homogeneous mixture, (b) $t=4.36$ s, (c) $t=9.36$ s, (d) $t=16.28$ s, (e) $t=23.2$ s, and (f) $t=40.68$ s. The snapshots corresponds to a central (73.1×59.5) mm^2 visualization window of the full tray.

In summary, the control parameters of the experiment were the amplitude A and frequency f of the applied vibration, the total filling fraction of the mixture, C, and the aspect ratio of the container, Γ.

III. THE SEGREGATION PROCESS

In our previous work [33–36] we presented experimental evidence for three qualitatively distinct phases of the binary mixture of poppy seeds and phosphor-bronze spheres. Each exists over a range of the filling fraction of the granular layer, C. We identified these phases as *binary gas* (unsegregated), *segregation liquid*, and *segregation crystal* [35].

The *binary gas* phase is found at low values of C and is essentially a collisional regime. In this phase there is enough free area and agitation such that the particles move randomly around the layer and a mixed state persists. In the *segregation liquid* phase, at intermediate values of C, aggregation of the phosphor-bronze spheres occurs and mobile liquidlike clusters form. A representative segregation pattern of the mixture in this segregation liquid phase is shown in Fig. 1(b). The snapshot corresponds to a segregated state which self-organizes after the mixture is vibrated for a period of 3 min, with forcing parameters $A=\pm 1.74$ mm and $f=12$ Hz

and aspect ratio $\Gamma=2$. The movement of the segregation domains is reminiscent of oil drops on water. The motion of the particles within the clusters is highly agitated and the collective motion is slow with merging and splitting of the domains.

The transition from the *binary gas* to *segregation liquid* phase [34] has the characteristics of a continuous phase transition with square-root dependence of the saturation levels as measured by the average stripe width which we treat as an order parameter. This critical phenomenon implies the existence of a transition point at $C_c \sim 0.65$, below which the layer remains mixed and above which segregation occurs. Moreover, critical slowing down of the segregation times scales is found near C_c.

At high filling fractions, for $C>0.89$ a second qualitative change of the structure and dynamics of the domains occurs as well-defined striped patterns, perpendicular to the direction of forcing, self-organize from the initial homogeneous mixture. We denote this third regime by *segregation crystal*. The near monodispersity of the phosphor-bronze spheres means that the segregation domains in this phase consist of particles disposed in a hexagonally packed lattice whereas the polydisperse poppy seeds always move around randomly.

A time sequence which is typical of the behavior seen at high filling fractions where crystalline stripes form, is presented in Fig. 2, for $C=0.996$. Immediately after the vibration is applied, single large particles diffuse in a sea of the smaller ones, exploring different local configurations. When two large particles happen to come close together, the smaller particles cannot fit between them, and hence the pair is subjected to an asymmetric pressure that keeps it together. Subsequently, pairs may encounter others so that progressively larger clusters form. The unidirectionality of the driving induces an asymmetry in the segregated domains such that elongated domains of the larger phosphor-bronze spheres develop in a direction which is orthogonal to the direction of the drive. During this initial period, the rapid formation of clusters suggests an effective attractive force between the phosphor-bronze spheres that leads to aggregation. Eventually, long domains form in the y-direction and well-defined stripes grow across the full width of the tray. This self-organization into segregation domains occurs within time scales of tens of seconds. For longer time scales of the order of a few hours, these segregated domains progressively coarsen with time, thereby merging to form increasingly robust stripes. The width of the domains follows a $t^{1/4}$ power law with time and this scaling is independent of the mixture used [33]. The coarsening takes place most obviously for values of C in the range ~ 0.1 to 0.2 above C_c. An extensive parametric investigation of the coarsening behavior as a function of C has yet to be carried out.

It is important to stress once more that, depending on the control parameters, the mixture does not always evolve into a robust striped pattern. This was only the case for filling fractions with $C>0.89$. At lower filling fractions, in particular closer, but above, to the segregation transition point C_c the segregated domains are increasingly mobile and bloblike, as shown in the representative liquid state of Fig. 1(b).

IV. VORONOI MEASURES

We now focus on the description of the segregation in our granular mixture using a number of *microscopic* measures. By microscopic, we mean that both structural and dynamical quantities are analyzed using the positions of the centers of the individual phosphor-bronze spheres obtained from the particle tracking analysis. This is by way of contrast with the macroscopic average width of the segregated domains and respective fluctuations used in our previous work [34–36].

The construction of Voronoi cells through tessellation (also know as Wigner-Seitz cells) is a standard tool for the study of spatial configurations of particle ensembles which is widely used in condensed matter physics [37] and is outlined as follows. Consider a set **P** of N coplanar particles with their centers located at $C_i(x,y)$ for $i=1 \rightarrow N$. For each particle i, Voronoi tessellation yields a polygonal cell that encloses a region inside which at any point is closer to the center C_i of the ith particle than any other in the set **P**. We have used the `voronoi (x,y)` routine in the package MATLAB 7.0 to implement this procedure. It is straightforward to extract a measure of the local area density associated with each phosphor-bronze sphere for this geometrical construction. It is also possible to obtain another useful measure of the angle between nearest neighbors. These two quantities are introduced in the following two sections, IV A and IV B, respectively.

A. Local Voronoi density

The first quantity considered is a measure of the *local area density* associated with each phosphor-bronze sphere [35]. Following a standard procedure [38], the *local Voronoi area density* of the ith sphere of an individual video frame can be defined as the ratio

$$\rho_v^i = \frac{A_{sphere}}{A_{cell}^i}, \tag{2}$$

where $A_{sphere}=\pi(d/2)^2$ is the two-dimensional projected area of the imaged spheres with diameter d and A_{cell}^i is the area of its Voronoi polygon.

In Fig. 3 we present examples of typical Voronoi configurations, at four different values of C, constructed using the positions of the phosphor-bronze spheres. In the binary gas regime at $C=0.495$ no segregation occurs and the network of Voronoi polygons appear random, as shown in Fig. 3(a). By way of contrast, at $C=1.007$ where definite segregation develops, structure appears in the domains as can be seen in Fig. 3(d). Two snapshots of the network of Voronoi cells for intermediate values of C are presented in Figs. 3(b) and 3(c). Note that the particles at the edges of the segregation clusters have an associated area density significantly lower than those in the bulk of the domains.

We first discuss the time evolution of the local Voronoi area density from the initial mixed state. A time window of $\Delta\tau=4$ s, which corresponds to 100 video frames (i.e., ~ 48 drive cycles) has been used to obtain dynamic averages for the area density of individual spheres, ρ_v^i, as,

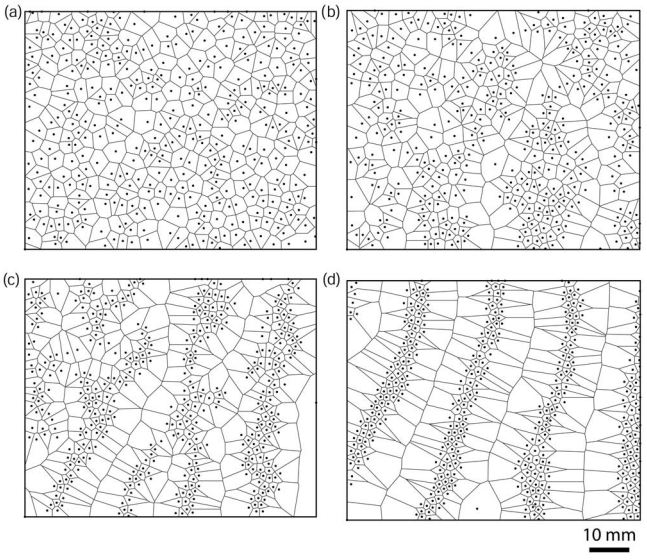

FIG. 3. Voronoi diagrams obtained from the positions of the phosphor-bronze spheres, for binary mixtures with various filling fraction values: (a) $C=0.495$, (b) $C=0.623$, (c) $C=0.687$, and (d) $C=0.751$. The frames correspond to configurations obtained 40 s after vibrating an initially homogeneous mixture.

$$\overline{\rho_v}\left(t_n=\frac{n\Delta\tau}{2}\right)=\langle\rho_v^i\rangle_n, \tag{3}$$

where the brackets $\langle\cdot\rangle_n$ denote averaging over all the particles, i, found within the nth time window, $n\Delta\tau<t_n<(n+1)\Delta\tau$ with $n\in[0,1,2,3,\ldots,59]$. A time dependent probability distribution function for the local Voronoi area density, $f_{PDF(\overline{\rho_v},t_n)}$, was obtained by constructing normalized histograms of $\overline{\rho_v}$ as a function of the discretized time, t_n. Each $f_{PDF(\overline{\rho_v},t_n)}$, for any time window n, typically contained statistical ensembles with 35,000 to 40,000 particles.

In Fig. 4 we plot the mean value of the distribution $f_{PDF(\overline{\rho_v},t_n)}D_v(t_n)$, for three values of the filling fraction. Let us

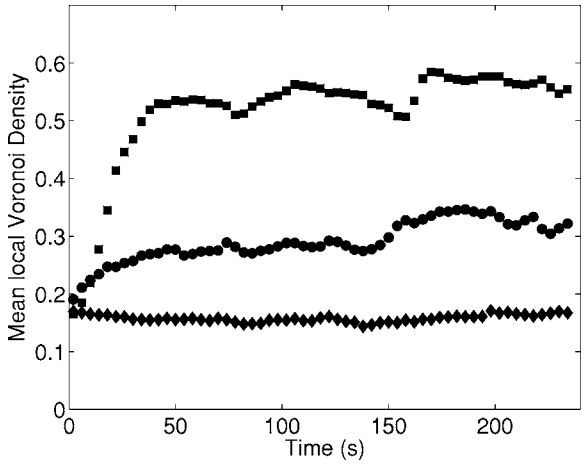

FIG. 4. Time evolution of mean local Voronoi area density, $D_v(t)$, having started from initially homogeneous mixtures. (♦) $C=0.495$, (●) $C=0.687$, and (■) $C=1.049$.

first focus on the behavior at early times, i.e., within the period $t\lesssim 100$ s. At $C=0.495$, $D_v(t_n)$ is flat since the layer remains mixed. At intermediate values of C, where $C=0.687$ is a typical example, $D_v(t_n)$ exhibits a slow increase up to a value of $D_v(t_n)\sim 0.3$ as segregation clusters form. At high values of filling fraction, of which $C=1.049$ is representative, there is a rapid initial evolution, since increasingly dense clusters form, up to a value of $D_v(t_n)\sim 0.525$ after which the mean area density levels off. This behavior is consistent with the observation of saturation in the macroscopic mean stripe width presented in our previous work [34–36].

At later times, i.e., $t\gtrsim 100$ s, the mean Voronoi area density for the two cases of $C=0.687$ and 1.049 only shows small deviations from the level off value of $D_v(t_n)$ and the system has reached a segregated state with a characteristic Voronoi density. The small dips in $D_v(t_n)$ correspond to the long term splitting and merging of stripes mentioned in Sec. III. An error estimate of the closeness to a steady state can be obtained from the ratio of the standard deviation to the mean of $D_v(177<t<233$ s), which was below 6.5% for all values of filling fraction considered.

The dynamical behavior of the segregation process can now be analyzed as a function of the filling fraction using the local Voronoi density. We focus on the initial stages of the formation of domains. During this regime of fast initial segregation growth, D_v exhibits an approximately linear behavior of the form

$$D_v(C,t)=D_v(t=0)+b(C)t, \tag{4}$$

where $D_v(t=0)$ is the mean area density of the initial homogeneous mixture and $b(C)$ is the corresponding *rate of segregation*. Three representative fits of this form are shown in Fig. 5 (inset) for the three experimental runs presented in Fig. 4 (with filling fractions $C=0.495$, 0.687, and 1.049). We stress that this linear description is certainly not valid across the full segregation growth regime but it provides us with an estimate of the initial rate (slope) of the dynamics, as the layer evolves away from the initially mixed conditions. A value of $D_v(t=0)=0.158\pm0.004$ provides a good fit to all experimental runs since the layer is consistently started from a homogeneous mixture. The inverse of the rate of segregation yields a measure of the segregation time scale, $t_D(C)=1/b(C)$, which is plotted in Fig. 5. This segregation time scale rapidly increases as C_c is approached from above. This result indicates that the dynamics of the segregation slow down near the segregation transition and it provides further evidence for the critical slowing down obtained from macroscopic measures in our own previous work [34,36]. However, in this case, it has been obtained from the statistics of the positions of individual particles.

In [35] we showed that the behavior of the probability distribution function $f_{PDF(\rho_v)}$ distributions obtained in the steady state regime (i.e., after the initial segregation growth) is useful in the characterization of the segregation in a mixture. At low values of C, the PDFs are peaked at small ρ_v. As C is increased a qualitative change in the shape of the PDFs is seen and at $C\sim 0.65$ they flatten out indicating that there is a greater probability of finding particles with an area density

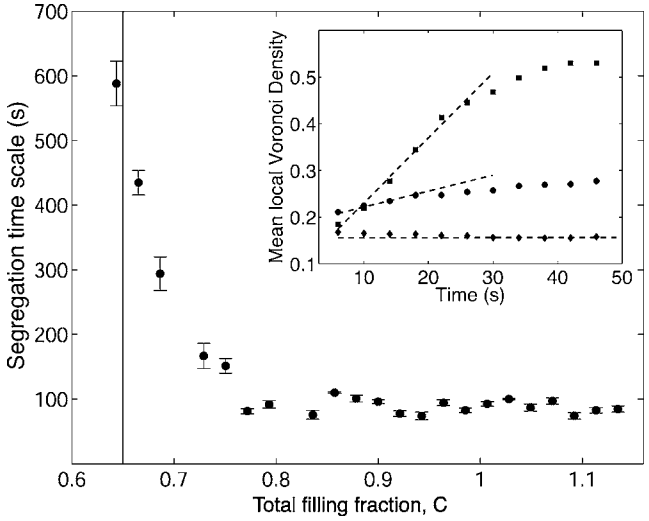

FIG. 5. Segregation time scale, $t_D=1/b(C)$ of the phosphor-bronze spheres as a function of filling fraction. The solid vertical line is positioned at the critical point for segregation, $C_c=0.650\pm0.043$, as obtained in Sec. IV A Inset: Detail of the time evolution of the mean local Voronoi area density, $D_v(t)$, with corresponding linear least-squares fits at early times, for three values of filling fraction—(♦) $C=0.495$, (●) $C=0.687$, and (■) $C=1.049$—from which an estimation of the segregation time scale, $t_D(C)$, is calculated.

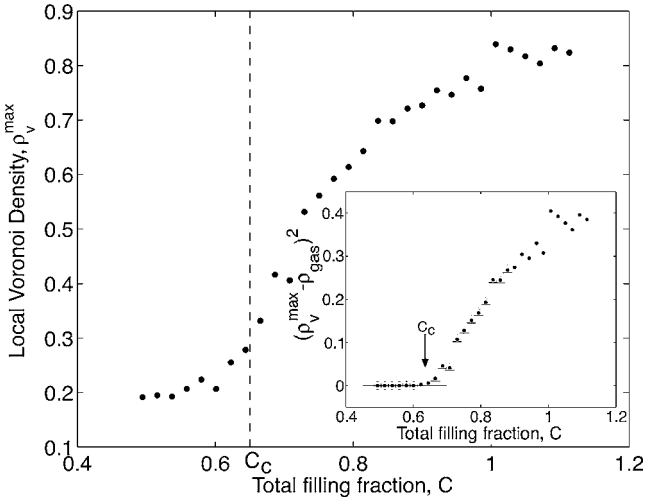

FIG. 6. Characteristic Voronoi density, $\rho_v^{\max}$, as a function of filling fraction C. The dashed vertical line is location at C_c. Inset: Squared data, $(\rho_v^{\max}-\langle\rho_{gas}\rangle)^2$, after subtracting level $\langle\rho_{gas}\rangle$ (as defined in the text). Linear least-squares fits were done for the two distinct regions with circles (solid line) and triangles (dashed line), respectively, the intercept of which yielded the binary gas to segregation liquid transition point C_c.

across the entire range. As C is increased further, a new peak develops at high area densities corresponding to particles within the segregation clusters. This peak at high ρ_v becomes increasingly sharper for high C, with a drop at values of $\rho_v=0.9$, which is consistent with maximum packing in 2D of $\pi/\sqrt{12}$ for a perfect hexagonal arrangement of disks.

The value of the median of the $f_{PDF(\rho_v)}$ distributions, ρ_v^{max}, measures the characteristic Voronoi density of the spheres in the mixture. The dependence of ρ_v^{max} on filling fraction is shown in Fig. 6. When the transition from binary gas to segregation liquid occurs by increasing C, ρ_v^{max} grows rapidly but continuously and segregation domains form. To numerically determine the location of the transition point C_c we have subtracted the base level value of $\langle\rho_{gas}\rangle=0.203\pm0.012$ to ρ_v^{max}, to obtain $(\rho_v^{max}-\langle\rho_{gas}\rangle)^2$, which is plotted in the inset of Fig. 6 (the brackets $\langle\cdot\rangle$ signify averaging of ρ_v^{max} in the range $C<0.623$). This quantity exhibits two linear regions, the intercept of which yields the transition point $C_c=0.650\pm0.043$, and sets the phase boundary between the mixed binary gas and the segregation liquid phases. The location of this phase boundary is in good agreement with the value of 0.647 ± 0.049 obtained from macroscopic measures (mean width of domains) in our previous work [34]. C_c will be used in Sec. V to aid mapping out the phase diagram of the granular mixture.

B. Angle between nearest neighbors

Another quantity that can be calculated from the Voronoi tessellation procedure is the angular distribution between nearest neighbors of each sphere. The configuration of a section of a schematic Voronoi polygon for a particle with coordinates $\mathbf{C}_i$ and two of its nearest neighbors, **A** and **B**, is given in the inset of Fig. 7. We define δ_i to be the angle between nearest neighbors set by **A**, **B**, and $\mathbf{C}_i$. This can be obtained from the Voronoi tessellation procedure which yields the position of the coordinates of the vertices of the Voronoi polygon $\mathbf{V}_1$, $\mathbf{V}_2$, and $\mathbf{V}_3$. Hence it follows from the geometric construction around the ith particle that

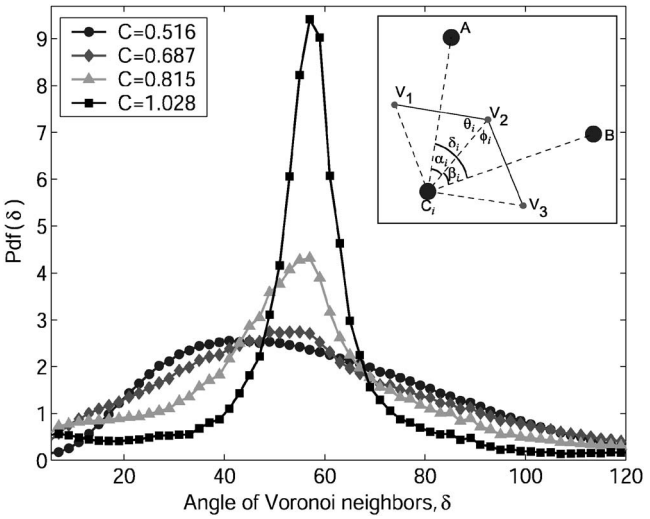

FIG. 7. Probability distribution functions for the angle between nearest neighbors, $f_{PDF(\delta)}$: for (●) $C=0.516$, (♦) $C=0.687$, (▲) $C=0.815$, and (■) $C=1.028$. Inset: Schematic diagram for the definition of angles between nearest neighbors, δ. **A**, **B**, and $\mathbf{C}_i$ are the positional coordinates of three neighboring particles. The angle defined by the three particles, about $\mathbf{C}_i$, is $\delta_i=\alpha_i+\beta_i$. The solid lines are a section of the Voronoi polygon, belonging to the particle $\mathbf{C}_i$, which is defined by the vertices $\mathbf{V}_1$, $\mathbf{V}_2$, and $\mathbf{V}_3$.

$$\delta_i = \alpha_i + \beta_i = 180 - (\phi_i + \theta_i) \tag{5}$$

where

$$\theta_i = \cos^{-1}\left(\frac{(\mathbf{V}_1 - \mathbf{V}_2)(\mathbf{C}_i - \mathbf{V}_2)}{|\mathbf{V}_1 - \mathbf{V}_2||\mathbf{C}_i - \mathbf{V}_2|}\right) \tag{6}$$

and

$$\phi_i = \cos^{-1}\left(\frac{(\mathbf{V}_3 - \mathbf{V}_2)(\mathbf{C}_i - \mathbf{V}_2)}{|\mathbf{V}_3 - \mathbf{V}_2||\mathbf{C}_i - \mathbf{V}_2|}\right). \tag{7}$$

Curves of the probability distribution function of the δ angles, $f_{PDF(\delta)}$, are presented in Fig. 7 for four representative values of C. For example, for small C the distribution is broad which indicates that the spheres do not exhibit a preferred orientation as expected for a mixture. However, as the filling fraction is increased the main peak of the distribution shifts towards 60° and the width of the peak decreases significantly. From the $f_{PDF(\delta)}$ distribution, we can now extract the location, δ^{max}, of its peak which measures the characteristic angle between nearest neighbors and the peak's width at half maximum, w, which yields information on the associated fluctuations. The latter is particularly useful in determining the boundary between the segregation liquid and segregation crystal phases.

The characteristic angle δ^{max} is plotted in Fig. 8(a). At the lowest values of C, δ^{max} tends to 45°. However, as C was increased, δ^{max} follows a nonmonotonic variation, as the mixture goes through the segregation transition. The characteristic angle first decreases to ~43.0° and then sharply increases after the segregation transition point. The nature of this nonmonotonic dependence of δ^{max} on C remains unclear. At the highest values of C the phosphor-bronze spheres self-organize into a nearly hexagonal pack, for which one would expect $\delta^{max}_{hex}=60°$. This is consistent with the value of $\delta^{max}=(57\pm2)°$ attained in the experiment at high C.

In Fig. 8(b) we present the filling fraction dependence of the width at half maximum, w, of $f_{PDF(\delta)}$. At low C, the distributions are broad, indicating that a wide range of angles between nearest neighbors is possible. This is consistent with a *binary gas* since there is no order. Near $C\sim0.65$, the point at which the segregation transition occurs, there is a quantitative change of behavior and w rapidly drops with increasing C. This region corresponds to the *segregation liquid phase*. This drop eventually levels off at high filling fractions, past a point $C_m=0.87\pm0.08$. We have identified C_m as a phase boundary between the segregation liquid and segregation crystal phases and numerically determined it from the intercept of linear least-squares fits to each of the two distinct regions at intermediate and high filling fractions. The boundaries of these two regions used in the fits are shown in the plot as triangles and squares, respectively. C_m will be used in Sec. V to aid mapping out the phase diagram of the granular mixture.

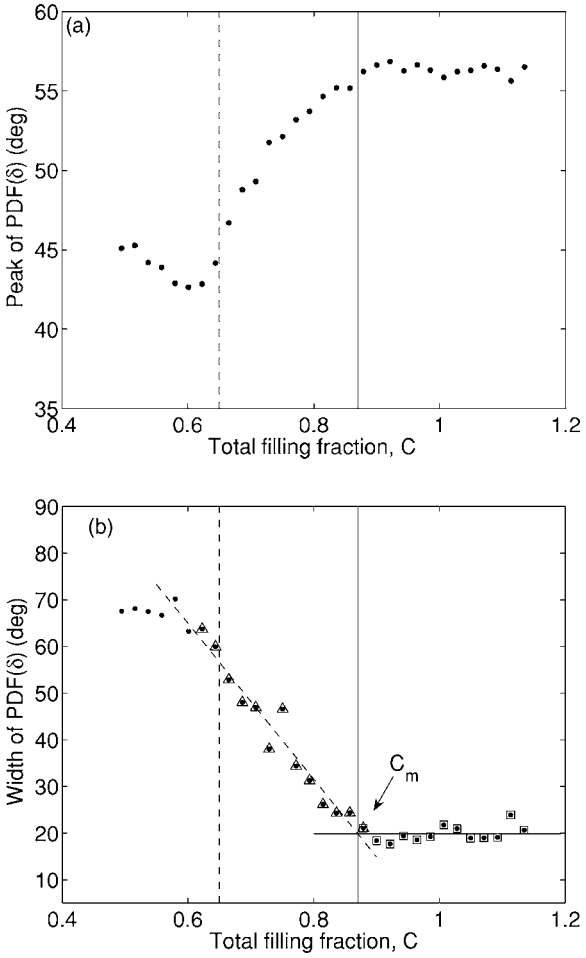

FIG. 8. (a) Location, $\delta^{\max}$, of the $f_{PDF(\delta)}$ distribution's peak. (b) Width at half maximum, w, of the $f_{PDF(\delta)}$ distribution's peak. The dashed vertical line represents the transition from binary gas to segregation liquid located at $C_c=0.650\pm0.043$, as determined in Sec. IV A. The vertical solid line represents the phase boundary between segregation liquid and crystal located at $C_m=0.87\pm0.08$. The oblique dashed and horizontal solid lines are the least-squares fits to the regions with triangles and squares, respectively.

V. EXPLORATION OF PARAMETER SPACE

A. Aspect ratio

We note that the segregation process appears to be independent of the shape of the boundaries. For example, we have performed experiments on a tray with circular boundaries and the dynamics of segregation were qualitatively identical to the rectangular case. It is now of interest to quantify the effect of varying the total area and aspect ratio of the tray, since C is a dimensionless ratio between the total projected area occupied by all the particles and the *area xy of the tray*. We focus on the case of rectangular boundaries. A frame with movable walls in both x and y was used to accomplish this. Its sidewalls were mounted in precision machined parallel grooves and the respective dimensions adjusted using a Vernier scale which was accurate to within ±0.05 mm. The range of the aspect ratio explored was $0.22<\Gamma<9.00$. The filling fraction of the layer was fixed at $C=0.900$ with $\varphi_{pb}=0.174$ phosphor-bronze spheres. Since the total area of tray varied while changing Γ, both N_{ps} and N_{pb} had to be changed accordingly in order to keep C and φ constant. The forcing parameters, as before, were set at $f=12$ Hz and $A=\pm1.74$ mm.

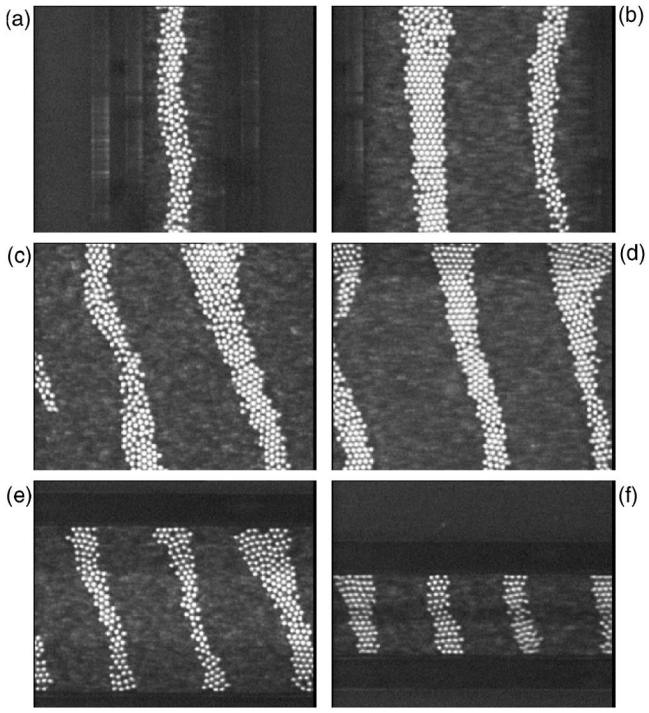

FIG. 9. Snapshots of the segregated phase for various values of Γ. The images correspond to the layer configuration 2 min after vibrating an initially homogeneous mixture with the following parameters: $C=0.900$, $\varphi_{pb}=0.174$, $f=12$ Hz, and $A=\pm 1.74$ mm. (a) $\Gamma=0.222$, (b) $\Gamma=0.667$, (c) $\Gamma=1.556$, (d) $\Gamma=2.571$, (e) $\Gamma=4.500$, and (f) $\Gamma=9.000$. The end-wall boundaries can be seen as dark vertical bands in (a) and (b) and the sidewalls as horizontal bands in (e) and (f).

Example snapshots of the granular layer taken after 2 min of vibration of an initially homogeneous mixture are presented in Figs. 9(a)–9(f), for various values of Γ. Note that the photographs correspond to a central imaging window of the full tray (73.1×59.5 mm^2) and hence in all experimental frames of Fig. 9 only a portion of the granular layer is shown. The vertical boundaries of the tray are, therefore, only observable in Figs. 9(a) and 9(b) and the horizontal boundaries in Figs. 9(e) and 9(f).

For $\Gamma \ll 1$, of which the frame in Fig. 9(a) is a representative example, a single stripe formed perpendicular to the direction of forcing. For larger values of Γ, a number of similar well-defined vertical stripes rapidly developed in the same way of the particular case of $\Gamma=2$, which was studied in detail in Secs. III and IV B. Moreover, the number of stripes in the system increased as Γ was increased. For example, increasing the tray's aspect ratio from $\Gamma=0.222$ [Fig. 9(a)] to $\Gamma=0.667$ [Fig. 9(b)] resulted in an increase from one to two stripes.

Even if a larger number of stripes could be attained by varying Γ, in all cases the stripes had a similar form, i.e., they had approximately the same longitudinal width even if their transverse height (set by Δy of the tray) decreased with Γ.

To further quantify this, we measured the characteristic local Voronoi area density of the spheres, ρ_v^{max} (introduced in Sec. IV A) as a function of Γ, the results of which are presented in Fig. 10.

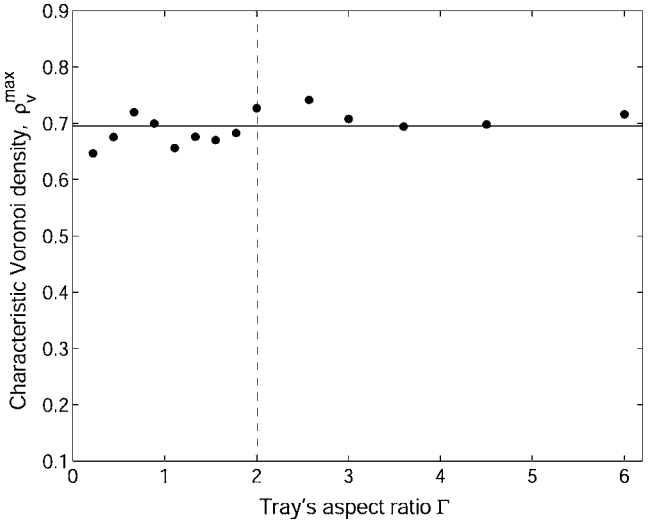

FIG. 10. Characteristic local Voronoi area density, $\rho_v^{\max}$, as a function of aspect ratio Γ. The mean value is $\langle \rho_v^{\max} \rangle_\Gamma = 0.696 \pm 0.040$, represented by the horizontal solid line. The vertical dashed line is located at $\Gamma=2$, corresponding to the value of the aspect ratio used for all detailed studies in this investigation.

As the aspect ratio of the tray was changed, the local area density of the phosphor-bronze spheres remained approximately constant with an average value of $\langle \rho_v^{max} \rangle_\Gamma = 0.696 \pm 0.040$ (solid horizontal line in Fig. 10), to within 6%. This suggests that the segregation behavior appears to be independent of the tray's total area and aspect ratio. This finding is, in a way, surprising since the smallest dimensions of the trays considered, in the extreme values of $\Gamma=0.222$ and $\Gamma=9$, were only one order of magnitude larger than the size of the individual particles. Therefore one could expect the effect of the boundaries to be of considerable importance in those extreme situations of Γ, which does not appear to be the case.

B. Filling fraction parameter space

The majority of the experiments were performed by keeping the filling fraction of the phosphor-bronze spheres fixed at $\varphi_{pb}=0.174$, and incrementally increasing the filling fraction of the poppy seeds, φ_{ps}. Hence it is possible that the transition sequences might be caused by reaching a critical fill ratio of the domain. In order to make sure that this was not the case, a series of experiments were performed where the dependence of the segregation transition on the relative composition of the binary mixture was investigated, while keeping the C constant. The amounts of spheres and poppy seeds, set by φ_{pb} and φ_{ps}, were varied accordingly, with the constraint of keeping the total filling fraction of the layer fixed at $C=0.79\pm 0.06$. The mean longitudinal width, σ, of the domains of phosphor-bronze spheres has been used as the order parameter to measure the state of the system. Details concerning this measure can be found in [34,36]. A plot of σ vs φ_{pb} is given in Fig. 11 where it can be seen that for low values of φ_{pb} the mean domain width is $\sigma=3.23\pm 0.04$ mm. This corresponds to approximately two sphere diameters and

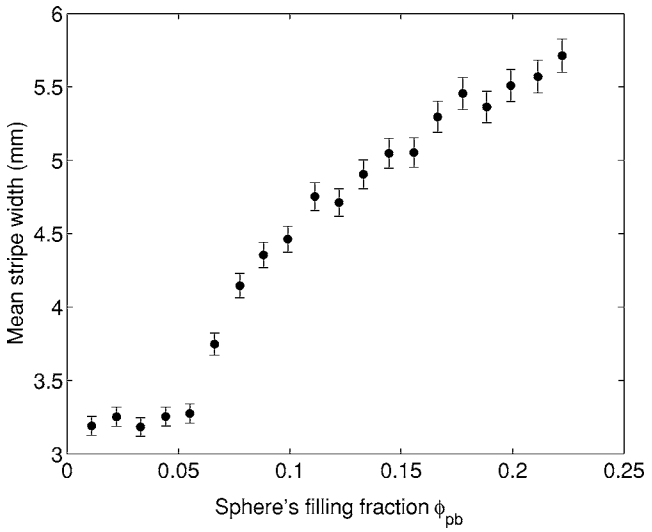

FIG. 11. Mean stripe width of spheres as a function of φ_{pb}. Total filling fraction was kept constant at $C=0.79\pm0.06$.

is consistent with the chance occurrence of neighboring particles averaged over the layer. Therefore these are not segregated domains and the layer is in a mixed state. As φ_{pb} is increased past $\varphi_{pb}^{c}=0.055$, σ increases continuously. We emphasize again that φ_{ps} has to be changed accordingly in order to keep C constant. This result suggests that, for segregation to occur, not only does the total filling fraction have to be large enough (i.e., above a critical value C_c as reported in [34]) but also the amount of spheres in the layer is required to be above a threshold value φ_{pb}^{c}. This result emphasizes the fact that the total filling fraction is a two-dimensional parameter $C(\varphi_{pb},\varphi_{ps})$.

Therefore the dependence of the segregation behavior on C was further explored in the *filling fraction parameter space*, $(\varphi_{ps},\varphi_{pb})$ by increasing the number of poppy seeds and hence scanning along φ_{ps} for four values of $\varphi_{pb}=\{0.054,0.083,0.118,0.174\}$.

The measure used to characterize the mixed-to-segregation transition with increasing C was the Voronoi area density, ρ_v^{max}, which was introduced and discussed in detail in Sec. IV A. The corresponding results are presented in Figs. 12(a)–12(d). All four data sets exhibit a clear transition between a mixed state (low area density) and segregated (high area density) state. A particularly interesting feature is that the transition becomes sharper in the mixtures with lower values of φ_{pb}. The mean value for the estimate of the mixed state at the left-hand edge of each graph is proportionally lower as φ_{pb} is decreased. This is expected since the overall area density of the phosphor-bronze spheres in the mixture is decreased, i.e., the total number of spheres in the tray is smaller for lower φ_{pb}. However, the branches corresponding to the segregated phases show no significant change at high C, for different φ_{pb}. Estimates of the local densities of $\rho_v\sim0.8$ were attained in all four cases, at the highest values of C. For $\varphi_{pb}=0.118$ we determined C_c in the same way to that of $\varphi_{pb}=0.174$ discussed in Sec. IV B. On the other hand the transition from mixed to segregated state for $\varphi_{pb}=0.083$ and 0.054 was sharp enough such that we took C_c as the highest C value in the mixed branch. The values of C_c for the four values of φ_{pb} are summarized in Table I.

The next two quantities that we shall discuss—the characteristic angle between nearest neighbors δ^{max} and width at half maximum extracted of the $f_{PDF(\delta)}$ distribution, w—have been introduced in Sec. IV B. In Figs. 12(e)–12(h) we present the results of δ^{max} for the four data sets with different φ_{pb}, plotted as a function of C. The behavior across the full range of C is qualitatively identical across all values of φ_{pb}. It is interesting to note that the nonmonotonic dependence of δ^{max} discussed previously appears to be robust as it is present in all four data sets. The nature of this effect is yet to be clarified.

The quantity, w, which is a measure of the fluctuations of $f_{PDF(\delta)}$, is plotted in Figs. 12(i)–12(l), for the four values of φ_{pb}. In all curves, three distinct regimes are evident where each corresponds to one of the phases of the binary mixture. This three step behavior in w can be seen in all four data sets confirming that the scenario of three segregation phases as a function of C is robust over a range of the filling fraction parameter space. As in Sec. IV B, we used w to determine the phase boundary C_m between the segregation liquid and the segregation crystal phases, the numerical values of which are presented in Table I.

In Fig. 13 the four data sets discussed thus far are combined in a $(\varphi_{ps},\varphi_{pb})$ phase diagram along with the phase boundaries C_c and C_m. The binary gas is located on the left-hand side of the diagram in the regions of low φ_{ps}. The segregation liquid exists in the central region of the diagram. The segregation crystal is observed at large values of φ_{ps}, on the right-hand side of the phase diagram. Note also that the phase boundaries $L1$ and $L3$ (dashed lines in Fig. 13) are alined and approximately parallel indicating that in this region of the phase diagram the total filling fraction is the primary parameter in determining the behavior, rather than the absolute amounts of each of the particle types.

We stress that strong deviations from the results presented here are to be expected in the limiting cases as the mixture approaches the single component regimes: (i) $\varphi_{pb}\to0$ and (ii) $\varphi_{ps}\to0$. Two sublimits of particular interest are those for the dense cases: (iii) $(\varphi_{pb}\to\sqrt{12}/\pi,\varphi_{ps}\to0)$ where crystallization of the phosphor-bronze spheres prevails and $(\varphi_{pb}\to0,\varphi_{ps}\to1)$ where the dense liquidlike nature of the poppy seeds dominates and segregation is suppressed. This is consistent with the polydispersity and shape of the poppy seeds preventing crystallization.

C. Forcing parameter space

In the results discussed thus far, the drive parameters were kept fixed at $f=12$ Hz and $A=\pm1.74$ mm. We now report the results of an investigation of the (f,A) parameter space. The aspect ratio and total filling fraction were fixed at $\Gamma=2$ and $C=0.900$ with $\varphi_{pb}=0.174$.

With $(f,A)=(12\text{ Hz},\pm1.74\text{ mm})$ the above conditions produced a dense segregation "liquid" from the initial mixture. However, all three phases can be obtained at appropriate locations in the (f,A) space. Examples of each of these phases can be seen in the experimental frames presented in

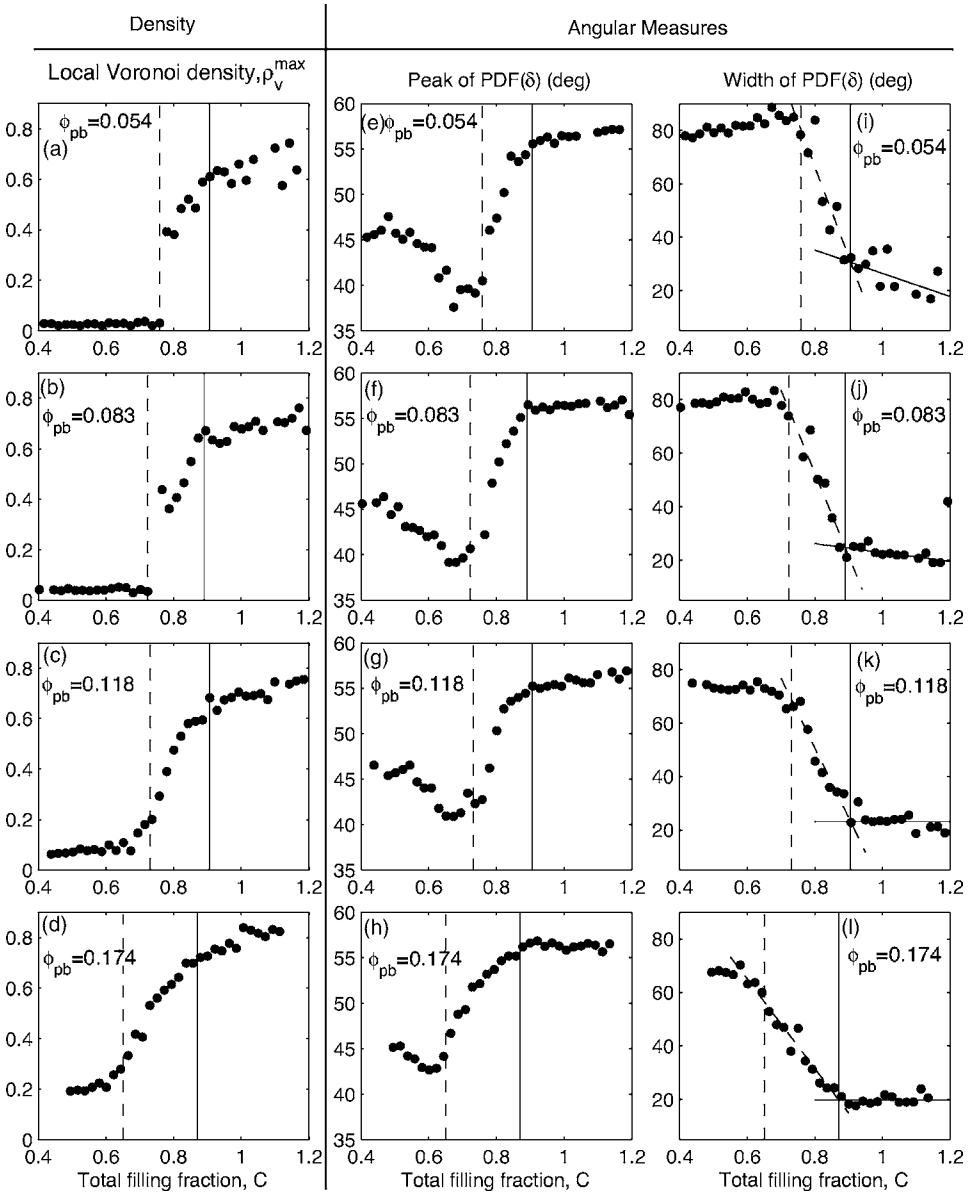

FIG. 12. Voronoi measures for the filling fraction phase space. First column: (a-d) Characteristic Voronoi area density. Second column: (e-h) Characteristic angle between nearest neighbors. Third column: (i-l) Width of the peak of the $f_{PDF(\delta)}$ distribution. The oblique dashed and horizontal solid lines are the least-squares fits to the respective intermediate and high filling fraction regimes, as discussed in Sec. IV B. The x-axis of all plots is the total filling fraction of the layer C with φ_{pb} set to (a, e, i) φ_{pb}=0.054, (b, f, j) φ_{pb} =0.083, (c, g, k) φ_{pb}=0.118, and (d, h, l) φ_{pb}=0.174. In each plot, the vertical dashed and solid lines are located at C_c and C_m, respectively, for that particular value of φ_{pb} (numerical values as in Table. I).

Figs. 14(a)–14(c). An example of a binary gas is shown in Fig. 14(a) for (f,A)=(28 Hz, ±1.18 mm). The forcing is sufficiently large to induce apparently random motion in the phosphor-bronze spheres across the layer and no segregation occurs. This example of a binary gas differs from the cases considered previously for $C<C_c$ in the sense that, at this high filling fractions (C=0.900), the particles in the layer have persistent contacts with their neighbors and there is only a small amount of free area in the tray. Therefore this is a highly agitated but noncollisional state. At (f,A) =(16 Hz, ±1.50 mm), segregation occurred and the segregation liquid shown in Fig. 14(b) was observed. An example of a segregation crystal is shown in Fig. 14(c) for (f,A) =(12 Hz, ±0.58 mm), where spheres within the domains were disposed in hexagonally packed configurations.

TABLE I. Numeric values for the binary-gas to segregation liquid transition, C_c, and for the segregation liquid to segregation liquid to segregation crystal transition, C_m.

φ_{pb}	C_c	C_m
0.054	0.758±0.021	0.906±0.236
0.083	0.723±0.021	0.890±0.128
0.118	0.731±0.067	0.906±0.118
0.174	0.650±0.043	0.870±0.080

The corresponding phase diagram for the (f,A) parameter space is presented in Fig. 14(d). Two clear examples of the segregation crystal phase were found at parameter values located in the lower right-hand corner of the diagram, i.e., for low amplitudes and frequencies. At intermediate values of the forcing, a segregation liquid phase was observed. At relatively large values of f and A segregation did not occur and a binary gas phase was dominant. The nature of the phase boundary between the segregation liquid and the binary gas phases [solid line in Fig. 14(d)] is discussed below.

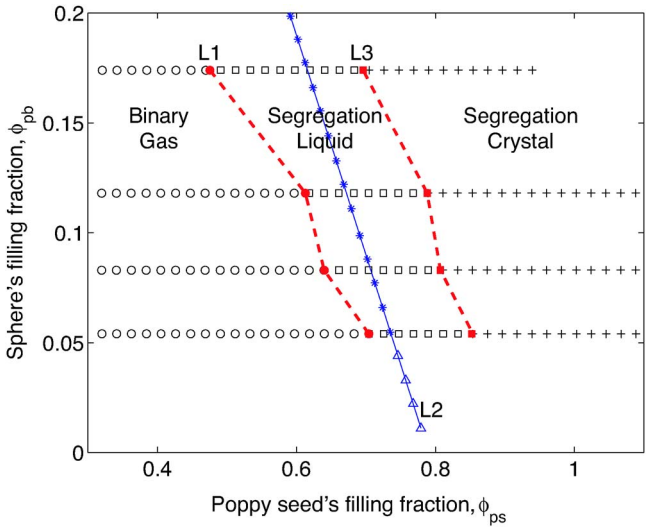

FIG. 13. (Color online) Phase diagram for the $(\varphi_{pb}, \varphi_{ps})$ parameter space. (○ and △) Binary gas. (□ and ∗) Segregation liquid. (+) Segregation crystal. The points along the oblique solid line, $L2$, correspond to the data presented in Fig. 11 for which the total filling fraction was kept constant at $C=0.79\pm0.06$ and the relative amounts of particles were changed accordingly (through φ_{pb} and φ_{ps}). The dashed lines, $L1$ and $L3$, are the experimental phase boundaries between the three phases of the mixture.

In order to obtain quantitative estimates of the behavior, the $f_{PDF(\rho_v)}$ of the distribution of the local Voronoi area density was calculated for each point in (f,A) space. The characteristic local Voronoi area density, ρ_v^{max}, was then obtained from the location of the maximum of the distribution, as before.

The dimensionless maximum acceleration of the tray is used to parametrize the forcing. It is given by

$$\gamma = 4\pi^2 \frac{Af^2}{g}, \tag{8}$$

where g is acceleration due to gravity. The parameter γ is commonly used in vertically vibrated granular systems [39] in which gravity plays a dominant role and the granular layer requires $\gamma > 1$ to leave the vibrating base. In our horizontal setup, gravity enters the problem indirectly through the frictional forces acting on individual particles, $F=\mu mg$ where m is the particle mass and μ its friction coefficient. In the ideal scenario of no rolling, the value of the nondimensional acceleration at which relative motion between the particle and the oscillatory tray appears would occur at $\gamma=\mu$.

In Fig. 15 the characteristic local Voronoi area density is plotted as a function of γ. All data points from the (f,A) parameter space study collapse on to a single curve, where two clearly distinct regimes can be observed. This indicates that γ is, indeed, an appropriate parameter to describe the forcing of the granular mixture through oscillatory motion of the tray.

At high accelerations, for $\gamma \gtrsim 3$, the characteristic Voronoi area density remains approximately constant with increasing γ. In this regime, the layer was in the highly agitated binary gas phase discussed above and no segregation occurred. As γ is decreased below $\gamma \sim 3$ the final state achieved becomes increasingly more dense in an approximately linear fashion. The solid and dashed lines in Fig. 15 were obtained from the best least-squares fits of the form $\rho_v^{max}(\gamma)=m\gamma+n$, in the region $0.34<\gamma<2.67$ (segregation phase) and $\rho_v^{max}(\gamma)=p$ in the region $3.34<\gamma<5.37$ (binary gas phase), respectively. The intercept of the two lines yields the location of the transition point which was measured to be $\gamma_c=2.95\pm0.16$

The relationship

$$f' = \frac{1}{2\pi}\sqrt{\frac{\gamma_c g}{A'}} \tag{9}$$

provides a good fit to the phase boundary, $f'(A')$, between the binary gas and segregation liquid phases as shown by the solid curve in Fig. 14(d). This also suggests that γ is the appropriate parameter to describe the forcing of the tray.

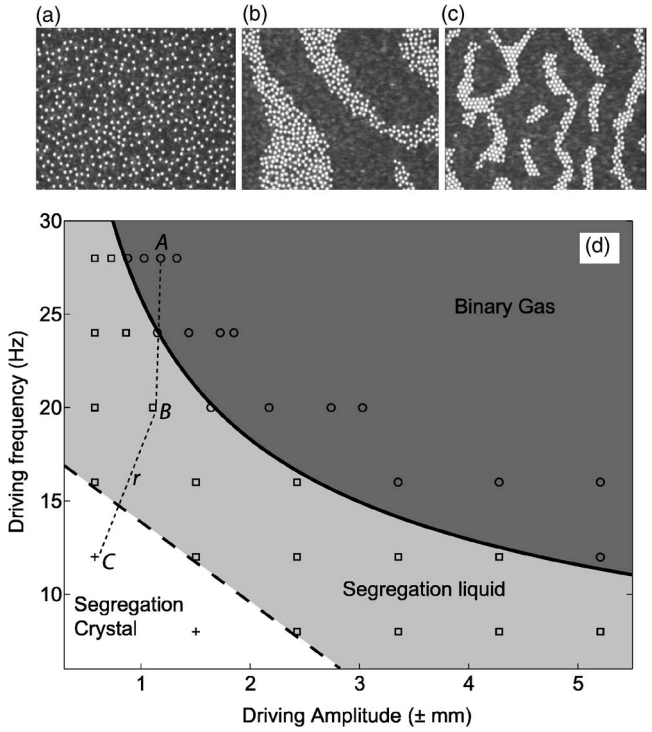

FIG. 14. Experimental frames of the binary mixture at various values of f and A. (a) Binary gas, $(f,A)=(28\ \text{Hz}, \pm 1.18\ \text{mm})$. (b) Segregation liquid, $(f,A)=(16\ \text{Hz}, \pm 1.50\ \text{mm})$. (c) Segregation crystal, $(f,A)=(12\ \text{Hz}, \pm 0.58\ \text{mm})$. $\Gamma=2$ $(\Delta y=180\ \text{mm})$ and $C=0.900$ with $\varphi_{pb}=0.174$. (d) Phase diagram for (f,A) parameter space showing regions of existence for the three phases. (○) Binary gas. (□) Segregation liquid. (+) Segregation crystal. The points A, B, and C, along the parameter path r, correspond to the experimental frames shown in (a), (b), and (c), respectively. The phase boundary between the segregation liquid and the binary gas phases is represented by the solid black curve and is given by Eq. (9) with $\gamma_c=2.95$.

VI. CONCLUSION

We have carried out a detailed experimental investigation of segregation behavior in a monolayer of two types of par-

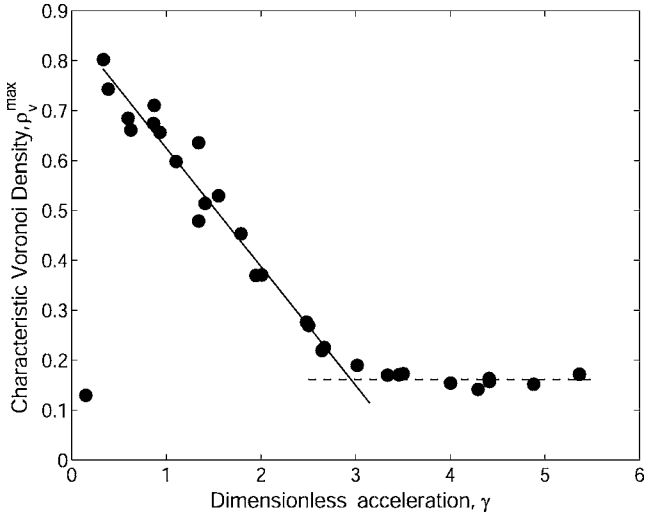

FIG. 15. Plot of the characteristic local Voronoi area density of individual spheres vs the nondimensional maximum acceleration γ for a range of values of (f,A). The transition is between a mixed (horizontal) and segregated (sloped) states. The solid and dashed lines are the best least-squares fit in the segregated and mixed regimes, respectively. The point with the lowest γ corresponds to a layer for which the forcing was insufficient to agitate the granular mixture.

ticles contained in a horizontal oscillating tray. The particles are set into motion via stick slip interaction with the base and this effectively randomizes their motion. An initially homogeneous mixed layer gives rise to spontaneous robust patterns when set into motion. The patterns have the form of clusters of one particle type and they persist over a wide range of the experimental conditions. The two principal control parameters of the system were found to be the layer filling fraction and the dimensionless acceleration of the driving. Moreover, we demonstrated that the essential mechanisms of the segregation process appeared to be independent of the aspect ratio of the tray.

Three qualitatively distinct phases were identified: a disordered binary gas for low values of C, segregation liquid with mobile domains of one of the particle types at intermediate values C, and segregation crystal where the domains are stripes oriented in a direction orthogonal to that of the driving at high values of C. Moreover, we have reported a transition between the segregated and mixed phases as the dimensionless acceleration of the driving was increased.

Recently, there has been a number of numerical studies where systems analogous to those of these experiments have been simulated [40–43]. The segregation behavior of these numerical systems is found to be in partial qualitative agreement with our experiments. Ciamarra *et al.* [42–44] have suggested that the segregation process is a result of dynamical instability which resembles the classical Kelvin-Helmholtz instability observed at a fluid interface. Similar stripe formation has also been observed in a continuum model of a binary fluid in which the components are differentially forced [40,45]. These studies suggest that the principal mechanism underlying segregation in this class of systems is the differential driving between each of the particle species. In our experiments, this could relate to the different surface properties of the phosphor-bronze spheres and the poppy seeds which induce different frictional interactions with the surface of the oscillatory tray.

However, even though the segregation patterns of the simulations are qualitatively similar to those observed in our experiments, none of the numerical models are as yet able to reproduce the critical behavior. In particular, there is no evidence for the associated critical slowing down of the dynamics near the transition region. Moreover, our parametric study of the driving parameters and the additional transition we have uncovered as a function of the dimensionless acceleration of the tray demonstrates that the forcing also plays a crucial role in the phase behavior of the granular mixture. This point has so far been overlooked in the numerical studies. We believe that this extensive investigation of the parameter space of our experimental system will be crucial for further testing and refinement of numerical models of the type mentioned above.

ACKNOWLEDGMENTS

P.M.R. was supported by the Portuguese Foundation of Science and Technology. The research of T.M. was supported by the EPSRC. The authors would like to thank D. Bonamy for advice on the Voronoi tessellation analysis and G. Ehrhardt for helpful discussions.

[1] H. Jaeger and S. Nagel, Science **255**, 1523 (1992).
[2] H. Jaeger, S. Nagel, and R. Behringer, Phys. Today **9**(4), 32 (1996).
[3] L. Kadanoff, Rev. Mod. Phys. **71**, 435 (1999).
[4] F. Melo, P. Umbanhowar, and H. L. Swinney, Phys. Rev. Lett. **72**, 172 (1994).
[5] B. Miller, C. O'Hern, and R. P. Behringer, Phys. Rev. Lett. **77**, 3110 (1996).
[6] D. Egolf, Science **287**, 101 (2000).
[7] T. Mullin, Science **295**, 1851 (2002).
[8] J. C. Williams, Powder Technol. **15**, 245 (1976).
[9] J. Bridgwater, in *Granular Matter* edited by A. Metha (Springer-Verlag, Berlin, 1993), p. 161.
[10] T. Shinbrot and F. Muzzio, Phys. Today **53**(3), 25 (2000).
[11] J. M. Ottino and D. V. Khakhar, Annu. Rev. Fluid Mech. **32**, 55 (2000).
[12] A. Kudrolli, Rep. Prog. Phys. **67**, 209 (2004).
[13] I. Aranson and L. S. Tsimring, Rev. Mod. Phys. **78**, 641 (2006).
[14] L. T. Fan, Y. Chen, and F. S. Lai, Powder Technol. **61**, 255 (1990).
[15] J. Bridgwater, Powder Technol. **15**, 215 (1976).

[16] J. C. Williams, Fuel Soc. J. **14**, 29 (1963).
[17] A. Rosato, K. J. Strandburg, F. Prinz, and R. H. Swendsen, Phys. Rev. Lett. **58**, 1038 (1987).
[18] J. Duran, J. Rajchenbach, and E. Clément, Phys. Rev. Lett. **70**, 2431 (1993).
[19] T. Shinbrot and F. J. Muzzio, Phys. Rev. Lett. **81**, 4365 (1998).
[20] M. Schröter, S. Ulrich, J. Kreft, J. B. Swift, and H. L. Swinney, Phys. Rev. E **74**, 011307 (2006).
[21] A. Betat, C. Dury, I. Rehberg, G. Ristow, M. Scherer, M. Schröter, and G. Straßburger, in *Evolution of Spontaneous Structures in Dissipative Continuous Systems*, edited by F. H. Busse and S. C. Muller (Springer, New York, 1998).
[22] B. Painter and R. P. Behringer, Phys. Rev. Lett. **85**, 3396 (2000).
[23] G. Metcalfe, S. G. K. Tennakoon, L. Kondic, D. G. Schaeffer, and R. P. Behringer, Phys. Rev. E **65**, 031302 (2002).
[24] S. Aumaitre, C. A. Kruelle, and I. Rehberg, Phys. Rev. E **64**, 041305 (2001).
[25] J. A. Drahun and J. Bridgwater, Powder Technol. **36**, 39 (1983).
[26] J. M. N. T. Gray and K. Hutter, Continuum Mech. Thermodyn. **9**, 341 (1997).
[27] J. P. Koeppe, M. Enz, and J. Kakalios, Phys. Rev. E **58**, R4104 (1998).
[28] P. Julien, Y. Lan, and Y. Raslan, in *Powder & Grains 97*, edited by R. Behringer and J. Jenkins (Balkema, Rotterdam, 1997).
[29] M. Donald and B. Roseman, Br. Chem. Eng. **7**, 749 (1962).
[30] E. Clément, J. Rajchencach, and J. Duran, Europhys. Lett. **30**, 7 (1995).
[31] K. M. Hill and J. Kakalios, Phys. Rev. E **52**, 4393 (1995).
[32] K. Choo, T. C. A. Molteno, and S. W. Morris, Phys. Rev. Lett. **79**, 2975 (1997).
[33] T. Mullin, Phys. Rev. Lett. **84**, 4741 (2000).
[34] P. M. Reis and T. Mullin, Phys. Rev. Lett. **89**, 244301 (2002).
[35] P. M. Reis, G. Ehrhardt, A. Stephenson, and T. Mullin, Europhys. Lett. **66**, 357 (2004).
[36] P. M. Reis, T. Mullin, and G. Ehrhardt, in *Unifying Concepts in Granular Media and Glasses*, edited by A. Coniglio, H. J. Herrmann, A. Fierro, and M. Nicodemi (Elsevier Science, Amsterdam, 2004), pp. 99–109.
[37] A. Okabe, B. Boots, and K. Sugihara, *Spacial Tesselations: Concepts and Applications of Voronoi Diagrams* (Wiley, New York, 1992).
[38] V. Kumar and V. Kumaran, J. Chem. Phys. **123**, 114501 (2005).
[39] F. Melo, P. B. Umbanhowar, and H. L. Swinney, Phys. Rev. Lett. **75**, 3838 (1995).
[40] C. M. Pooley and J. M. Yeomans, Phys. Rev. Lett. **93**, 118001 (2004).
[41] G. C. M. A. Ehrhardt, A. Stephenson, and P. M. Reis, Phys. Rev. E **71**, 041301 (2005).
[42] M. P. Ciamarra, A. Coniglio, and M. Nicodemi, Phys. Rev. Lett. **94**, 188001 (2005).
[43] M. Pica Ciamarra, A. Coniglio, and M. Nicodemi, J. Phys.: Condens. Matter **17**, S2549 (2005).
[44] M. Pica Ciamarra, A. Coniglio, and M. Nicodemi, Phys. Rev. Lett. **97**, 038001 (2006).
[45] P. Sánchez, M. R. Swift, and P. J. King, Phys. Rev. Lett. **93**, 184302 (2004).